 doi:10.20944/preprints202205.0136.v1

*Article*

# Cells-in-touch: 3D printing in reconstruction and modelling of microscopic biological geometries for research and education

**Xavier Fitzpatrick [1,2], Alexey Fayzullin [3,4], Socrates Dokos[2], and Anna Guller [1,25,*]**

[1] ARC Centre of Excellence for Nanoscale Biophotonics, Australia;xfitz97@gmail.com ; anna.guller@mq.edu.au
[2] The Graduate School of Biomedical Engineering, University of New South Wales, Sydney, NSW 2052, Australia; s.dokos@unsw.edu.au
[3] Institute for Regenerative Medicine, Sechenov First Moscow State Medical University (Sechenov University), Moscow, 119991, Russia; fayzullin_a_l@staff.sechenov.ru;
[4] World-Class Research Center "Digital Biodesign and Personalized Healthcare", Sechenov First Moscow State Medical University (Sechenov University), 119991 Moscow, Russia;
[5] Faculty of Medicine, Health and Human Sciences, Macquarie University, Sydney, NSW 2109, Australia.
* Correspondence: anna.guller@mq.edu.au

**Abstract:** Additive manufacturing (3D printing) and computer-aided design (CAD) still have limited uptake in biomedical and bioengineering research and education, despite the significant potential of these technologies. The utility of organ-scale 3D-printed models of living structures is widely appreciated, while the workflows for microscopy data translation into tactile-accessible replicas are not well developed yet. Here, we demonstrate an accessible and reproducible CAD-based methodology for generating 3D-printed scalable models of human cells cultured in vitro and imaged using conventional scanning confocal microscopy and fused deposition modelling (FDM) 3D printing. We termed this technology *CiTo-3DP* (**C**ells-**i**n-**To**uch for **3D P**rinting). As a proof-of-concept, we created CiTo-3DP models of human pancreatic cancer cells and healthy dermal fibroblasts by using selectively stained nuclei and the cytoskeleton components (f-actin and $\alpha$-smooth muscle actin). The production of dismountable sets of cellular components was also shown. The CiTo-3DP approach can be adapted to comprehensively present various cell types, subcellular structures and extracellular matrices. We envisage that the resulting CAD and 3D printed models could be used for further applications, including but not limited to in silico simulations for biology, medicine, pharmacological research, tissue engineering, morphometrical analysis, multiphysics modelling, education, rehabilitation of visually impaired people, and integration into virtual reality.

**Keywords:** 3D printing; microscopy; CAD; FDM; cell shape; cytoskeleton; tactile education; data visualization; modelling; Materialise Mimics; Cito-3DP.

## 1. Introduction

Additive manufacturing (AM), commonly termed as 3D printing [1], is a methodology of physical reconstruction of three-dimensional structures and complex geometries from digital models of these objects formed (in a core concept, and in contrast to the traditional subtractive or formative manufacturing approaches) by layered deposition of the material [2]. 3D printing has excelled as a disruptive technology in manufacturing in recent decades [3]. The success of AM may be attributed to its affordability, flexibility, safety and efficiency compared to more traditional manufacturing processes [4]. The most common modalities of 3D printing, in order of increasing spatial resolution capacity, include powder bed fusion (e.g., selective laser sintering, SLS), fused deposition modelling (FDM), the inkjet printing, and stereolithography (SLA) [1]. The availability of the affordable FDM desktop 3D printers and open-access processing software has made this technology truly global and friendly for the entry-level consumers [5].

 doi:10.20944/preprints202205.0136.v1

The workflow for most AM-technologies includes (1) computer-aided design (CAD) as a process of transforming the imaging data into a digital model representation of a 3D object, (2) model post-processing, or "slicing", and (3) printing [6]. There are several CAD options for reconstructing images into in silico 3D models in a stereolithographic format (STL), both commercial and open-access [7]. Open-access softwares for post-processing such as 3D Slicer and ImageJ are rapidly evolving too. However, currently, they are still outperformed by commercial softwares, such as the Mimics Innovation Suite (Materialise, Belgium), Simpleware (Synopsis, CA), and Amira (Thermo Fisher Scientific, MA), which offer faster, more powerful, and more user-friendly features [9]. There are several commercial options for 3D printing of stereolithographic (STL) format files using FDM, such as Ultimaker (Imaginables Pty Ltd, Melbourne Australia) and Makerbot (Makerbot Industries, NY). Further to this, various materials can be used for 3D printing, offering a range of textures, strengths and extrusion properties. The most common FDM printing materials are acrylonitrile butadiene styrene (ABS) and polylactic acid (PLA) filaments. These plastics are compatible with various FDM 3D printers, and similar in their performance and affordable cost [10], while PLA has much better safety profile than ABS [11].

Medicine and bioengineering are among the most promising areas of AM applications. In these fields, 3D printing relevance, to date, has been demonstrated mostly at the macro-scale, often utilizing rapid prototyping of structures visualized by computer tomography (CT) and magnetic resonance imaging (MRI) for individualized prosthetics [12,13], implants, and pro-regenerative scaffolds [2,14]. It is important to note that modern 3D printers have a higher isometric resolution (~100 μm) than CT or MRI scans (i.e., the CT pixel size is 0.15 - 0.5 mm and interslice distance is 0.4 - 1.0 mm), allowing a very detailed reproduction of various body structures [15]. Therefore, 3D printed patient-specific anatomical models provide an excellent opportunity for pre-interventional tactile and visual appreciation for surgical applications than it is possible from 2D CT or MRI images, for better operative planning, including choosing the appropriate implantable devices, and improvement of treatment outcomes [2,16-19].

Notably, 3D printing also offers an innovative and feasible way for introducing tactility into the educational curriculum, resulting in greatly improved learning outcomes by 3D printed models as tactile data visualizations [20]. For example, detailed 3D printed anatomical models of prosected organs allow replacement of several expensive and labor-intensive processes used in medical education [15]. In fact, 3D printed replicas provide a physical interface through which users can directly interact with the source data and get difficult scientific and engineering concepts in a more accessible way. Such approach reduces the cognitive load and improves the knowledge translation. 3D printed models also can enhance learning experience for visually impaired and disabled students, and for students with special needs [20].

Recently, AM has expanded into the realm of microscopy, both from the instruments' building [7] and the biological objects' physical reconstruction aspects [5,6,8,22-25]. In general, 3D printing of the microscopy-imaged structures follows the standard CAD-to-AM workflow. However, in contrast to the reconstruction of the objects visualized by CT and MRI, microscopy-to-3D printing relies on the source images with spatial resolution, which is higher than those achievable [15] by modern 3D printers. The spatial resolution for the light diffraction-limited imaging modalities is approximately 1 μm, while electron microscopy and super-resolution techniques allow depicting of nanoscale features. Importantly, the microscopy-to-3D printing workflow includes extra steps not only for recoding microscopy imaging data into STL format but also for rescaling the CAD model into a tactile-accessible size. An overview of the published data on the state-of-the-art approaches in 3D printing reconstruction of microscopic biological objects is shown in Table 1.

Preprints (www.preprints.org) | NOT PEER-REVIEWED | Posted: 10 May 2022 doi:10.20944/preprints202205.0136.v1

**Table 1.** 3D-printed models developed on the base of microscopic images of biological objects (literature analysis).

| AM parameter | Biological object | | | | | |
|---|---|---|---|---|---|---|
| | **Natural killer cell** | **Blood cells** | ***C. elegans* embryo and distal tip cell, a part of a plant cell** | **Pollen, blood cells, plant root, insect eye, zebrafish larva** | **Nucleus of a HeLa cell, pollen shells, fruit fly** | **Plant Golgi stacks** |
| Imaging modality[1] | STED | TEM | MPM, SCF, and TEM | SCF (all samples, except zebrafish larva) and LSHM (zebrafish larva) | SCF | TEM |
| Detected signals[2] | Phalloidin-Alexa Fluor 488 (f-actin) | SET | AF, gGFP | AF (all samples, except zebrafish larva), Phalloidin-FITC (f-actin), DAPI (omitted)* (zebrafish larva only) | DAPI (cell nucleus), AF (other objects) | SET |
| 3D reconstruction | Huygens, Imaris, Blender | AMIRA, IMOD, Rhinoceros 3D | Mimics, Geomagics | Bitplane Imaris, MeshLab | ImageJ 3D Viewer Plugin | IMOD, 3dmod |
| 3D printer | MakerBot Replicator 2X | FELIX 3.0 Dual Extruder | Spectrum Z510 | Zortrax M200 | UP Plus 2 | Lulzbot Mini and Form1+ |
| Printing software[3] | Makerware | Repetier-Host for FELIX Printers | Zprint Software | Zortrax Z-Suite | N.D. | N.D. |
| 3D printing technology[4] | FDM | FDM | IPT | FDM | FDM | FDM and SLA |
| Printing material[5] | ABS filament | PLA, PVA (support) | Plaster Powder | ABS filament | TP | TP and UR |
| References | [5] | [23] | [22] | [6] | [24] | [25] |

Abbreviations: AM – additive manufacturing; [1]: STED - Non-diffraction limited stimulated emission depletion microscopy, TEM – transmission electron microscopy, MPM – Multiphoton microscopy, SCF – scanning confocal microscopy, LSHM – lightsheet microscopy; [2]: SET – serial electron tomography; AF – autofluorescence, gGFP – genetically encoded green fluorescent protein, Phalloidin-FITC – phalloidin conjugated with fluorescein isothiocyanate; DAPI – 4′,6-diamidino-2-phenylindole, DAPI (omitted)* - zebrafish larva also was stained with DAPI, however, in the final visualization and 3D printed model the nuclear staining was omitted; DNA – desoxyribonucleic acid; [3] N.D. – no data provided; [4] – FDM – fused deposition modelling, IPT – inkjet printing technology, SLA - stereolithography; [5] – ABS - acrylonitrile butadiene styrene, PLA – polylactic acid, PVA – polyvinyl alcohol, TP – thermoplastic (unspecified), UR - unspecified resin.

As shown in Table 1, to date, the models of four classes of microscopic biological objects, such as (i) whole cells of mammalian and invertebrate origin, (ii) pollen, (iii) parts or clusters of the plant cells, and (iv) whole embryos of small laboratory animals have been 3D printed. Five imaging modalities were employed for the generation of the source images, including the stimulated emission depletion microscopy (STED) and serial electron tomography based on transmission electron microscopy (TEM), multiphoton microscopy, lightsheet microscopy and scanning confocal microscopy (SCM). Expectably, SCM is emerging as the most accessible imaging method that allows 3D virtual reconstructions,

 doi:10.20944/preprints202205.0136.v1

while FDM is becoming the most used printing modality in microscopy-to-3D printing modelling of biological objects.

Despite the fast development of this approach, it still has some substantial knowledge and methodological gaps. (1) Firstly, no microscopy-to-3D printing models of mammalian cells that form solid tissues have been shown yet. Also, there is still no comparative presentation of the different types of cells/ tissues of origin, health and disease state, embryonic origin, and functional polarization in 3D printed form. (2) Next, despite using different contrasting methods, no multiplexing of contrast agents have been employed in the published examples of the 3D printed models of biological microstructures. As a result, cumbersome manual procedures for the segmentation of the images were required to depict different subcellular structures in the same cells. (3) Finally, none of the published protocols allowed interactive dismountability. In simple words, this option allows to "assemble" or "disassemble" the "cell". Therefore, this is considered as an engaging interactive stimulus for better integrating 3D printed models in educational and, potentially, research contexts.

Here, we address the indicated challenges and present a proof-of-concept together with the practical protocols for the up-to-date methodology which we termed CiTo-3DP (**C**ells-**i**n-**To**uch for **3D P**rinting) for producing 3D PLA prints from SCM serial images (z-stacks) of two types of human cells: pancreatic cancer cells (cell line PANC-1) and primary healthy fibroblasts of skin derma. We simultaneously visualized subcellular structures including nuclei and two type of cytoskeletal elements (f-actin stress fibers and contractile $\alpha$-smooth muscle actin) using fluorescent contrasting agents with discernible spectral characteristics. Notably, an important marker of fibroblasts' phenotype conversion, the $\alpha$-smooth muscle actin ($\alpha$-SMA), was presented in 3D printed models for the first time. In the proposed workflow, we also demonstrated creation of the first 3D printed dismountable set of subcellular components, such as the cell nucleus and the cytoskeleton. Our report also provides rich research and educational context of the presented workflow (Appendix A, Section A1). The diversity of its future applications allowed because of the feasibility and adaptability of the CiTo-3DP approach is discussed.

## 2. Materials and Methods

### *2.1. Study Design*

The following method was designed to generate 3D cell reconstructions from immunofluorescent confocal z-stack images, optimized for 3D printing using commercially available FDM printers. The workflow applied in the current study is schematically shown in Figure 1. The presented method, which uses Olympus, Mimics and Ultimaker software and prints on Ultimaker hardware, allows fast extraction and analysis of meaningful biological information from routinely processed histological and in vitro cultured cells' samples. The detailed technical notes for the workflow presented here are provided in Appendix A, Section A2.

Preprints (www.preprints.org) | NOT PEER-REVIEWED | Posted: 10 May 2022 doi:10.20944/preprints202205.0136.v1

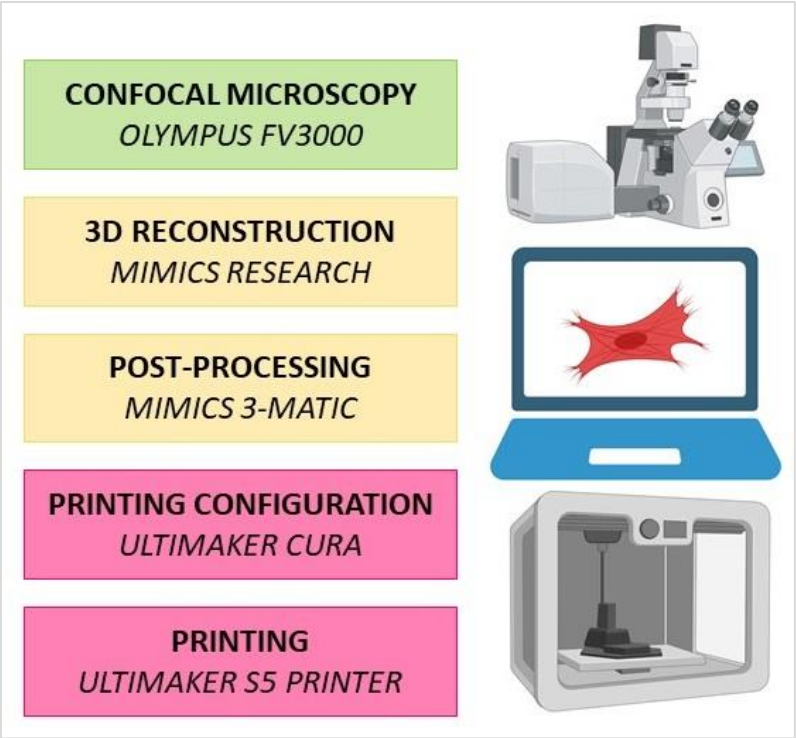


**Figure 1.** The workflow applied in the current study. Z-stacks of 2D cell images were acquired with an Olympus FV3000 confocal laser scanning microscope. Subsequently, CAD models of the cells were generated using Mimics research software. Post-processing was performed using Mimics 3-matic. Finalization of the model for printing was conducted using Ultimaker CURA. PLA models were printed with an Ultimaker S5 printer.

*2.2. Cell Culture and Staining Procedures*

Two cell types were used for the proof-of-concept of this methodology, including the primary healthy Human Dermal Fibroblasts (HDF, #106-05A, Sigma-Aldrich) and the tumour cell line PANC-1 which is representative for the human pancreatic adenocarcinoma (CRL-1469™, ATTC). HDF cells were cultured in Fibroblast Growth Medium (#116-500, Sigma-Aldrich) according to the recommended protocol [44]. PANC-1 cells were cultured Dulbecco's Modified Eagle's Medium (#11995, DMEM, high glucose, pyruvate, Thermo Fisher) with 10% fetal bovine serum (FBS) (#16000044, Thermo Fisher), 1% antibiotic-antimycotic (#A5955, Sigma-Aldrich, Australia) and 1% L-glutamine. Both cell types were cultured in Corning T-75 cell culture flasks (#CLS430641, Sigma-Aldrich) at 37°C with a 5% $CO_2$. Cells were passaged one-two times per week (after reaching 70-80% confluency) via detachment with Trypsin/EDTA solution (#T3924, Sigma-Aldrich).

For the imaging of the subcellular structures, cells were further cultured in 35 mm coverslip-bottomed culture dishes (#81156, Ibidi, Germany) overnight, and then washed with phosphate buffered saline (PBS; #D8537, Sigma-Aldrich) and fixed with 10% neutral buffered formalin (#HT501128, Sigma-Aldrich) for 20 min at room temperature. Following two washes with PBS, cellular nuclei were stained with NucBlue™ Fixed Cell ReadyProbes™ Reagent (DAPI) (#R37606, Thermo Fisher) and the f-actin filaments of the cytoskeleton were stained with Phalloidin-TRITC (#P1951, Sigma-Aldrich). The HDF samples were also stained with the mouse-anti-human α-SMA monoclonal antibody (#A2547, Sigma-Aldrich) and the donkey-anti-mouse secondary antibody Alexa Fluor Plus 647 (#R322787, Invitrogen). Stained cells were washed and stored in PBS at 4°C with the protection from visible light until imaging (24-48 h).

*2.3. Image Acquisition*

Preprints (www.preprints.org) | NOT PEER-REVIEWED | Posted: 10 May 2022 doi:10.20944/preprints202205.0136.v1

The cells were imaged using an Olympus FV3000 confocal laser scanning microscopy system equipped with Fluoview software (Olympus, Japan). The confocal microscopy settings used in this study are shown in Table 2.

**Table 2.** Confocal microscopy image acquisition settings.

| Settings | Subcellular structures | | |
|---|---|---|---|
| | **Nuclei (DNA)** | **F-actin** | **α-SMA** |
| Staining | DAPI | TRITC | Alexa Fluor 647 |
| Excitation laser, nm | 405 | 561 | 640 |
| Emission Filter (range), nm | 430-470 (DAPI) | 572-612 | 670-770 |
| Excitation maximum | 357 | 552 | 658 |
| Emission maximum, nm | 463 | 576 | 675 |

Table 3 describes the dimensions of the confocal microscopy images used. The final z-stack images were exported in Tagged Image File Format (TIFF) file format with imaging metadata stored as a text (.txt) file.

**Table 3.** Dimensions of the confocal microscopy images.

| Settings | Cell type | |
|---|---|---|
| | **PANC-1** | **HDF** |
| Image Size [pixels] | 1024 × 1024 | 1024 × 1024 |
| Objective | UPLSAPO 60× | UPLSAPO 20× |
| Numerical Aperture | 1.35 | 0.75 |
| Immersion media | PBS | PBS |
| Image Size (XY) [µm] | 212.132 × 212.132 | 636.396 × 636.396 |
| Voxel resolution (XYZ) [µm/pixel$^3$] | 0.207 × 0.207 × 1.000 | 0.621 × 0.621 × 0.500 |
| Number of z-slices | 16 | 33 |

*2.4. 3D Reconstruction*

As shown in Figure 2, the TIFF z-stack images were imported into a biomedical image segmentation software, Mimics Research 21.0 (Materialise, Belgium), typically used in 3D macro-anatomical analysis of DICOM images. It should be noted that image quality is the most important contributor to reconstruction accuracy. On import, image aspect and scale, in nm or µm, were validated against the coronal, axial and sagittal coordinate axes.

The main enabling tool used for 3D reconstruction of images was thresholding. The following workflow was applied: Thresholding (Tool: Segment > Threshold; or Tool: Segment > Dynamic Region Grow) inputs grey-scale, or "Grey Value" (GV), pixel-intensity maxima and minima, allowing for 3D image segmentation into new masks appearing in the software's Project Management and 3D previewer windows. New masks are comprised of tessellated mesh surfaces, wrapped around individual or adjacent image pixels. In this way, imported image stacks were organised into 3D reconstructions of isolated cellular components.

 doi:10.20944/preprints202205.0136.v1

Alternatively, cellular components were separated by splitting the mask (Tool: Split Mask). Following this, masks were cropped (Tool: Segment > Crop Mask; or Tool: Segment > Region Grow) to include only the information required. In cell-biology, single cells or smaller cellular clusters may be isolated in this way. The next step was to optimize the obtained 3D reconstruction for printing.

Due to the nature of immunofluorescent confocal microscopy as well as the nature of the imaged subcellular structures, where the cytoskeleton plays the role of the tension-bearing element for the outer cell membrane, there will be several holes in the reconstructed surface. For 3D printing using FDM technology, it is best to have a solid surface, as this will reduce printing time and cost. Therefore, the surfaces of the segmented masks were expanded by filling (Tool: Segment > Smart Fill) and brushing individual 2D images (Tool: Segment > Smart Fill > Local Fill). Any reconstruction errors inconsistent with the imaged biology, which may arise due to image resolution and thresholding, were erased by highlighting the respective region (Tool: Segment > Edit Masks).

Preprints (www.preprints.org) | NOT PEER-REVIEWED | Posted: 10 May 2022 doi:10.20944/preprints202205.0136.v1

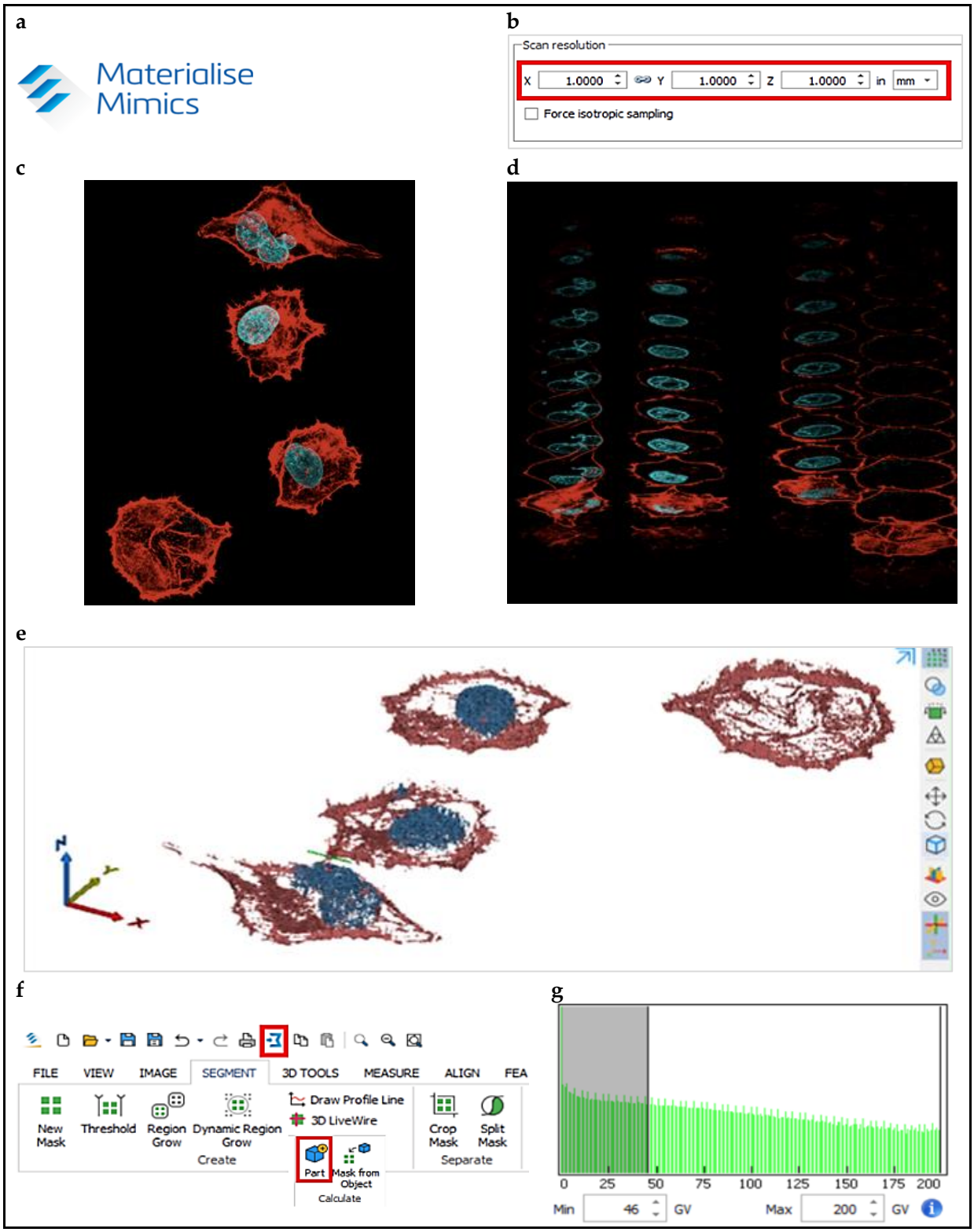


**Figure 2.** 3D reconstruction workflow. **(a)** Materialise Mimics software; **(b)** Mimics Research import voxel definition. Voxel dimensions are taken from the confocal imaging z-stack metadata; **(c)** Confocal microscope image of PANC-1 cells with the nuclei stained by DAPI (blue) and cytoskeletal f-actin filaments stained with phalloidin-TRITC (red); **(d)** An example of the individual images composing the z-stack of PANC-1 cells; **(e)** Segmented PANC-1 cell reconstructions generated from z-stack images (blue – nucleus, brown – f-actin cytoskeleton); (f) A screenshot of Materialise Mimics Research software toolbar with the "Create" part and part of "Export" tools highlighted; **(g)** Thresholding Grey Value (GV) histogram.

 doi:10.20944/preprints202205.0136.v1

*2.5. Post-processing*

Post-processing of meshed geometries, or parts, is an important step in 3D printing, as it prevents printing failure through further.

With the surfaces segmented and ready for post-processing, the relevant masks were converted into meshed geometries, or parts. The parts (Tool: Segment > Part) were exported into *Mimics 3-matic* software (Figure3). Note that *Mimics Research* works in the validated image scale, but *Mimics 3-matic* is constrained to operate in mm, with actual scale stored in memory. Although this scale transformation is automatic within the Materialise software, it was validated by measurement of key lengths in both softwares (Tool: Measure > Distance).

Imported parts, displayed in the software Object Tree, were colour coordinated (Tool: Object Tree > Object Properties > Colours) and aligned (Tool: Align) for improved workflow. To view object interiors, a viewing-plane was defined and translated through the object (Tool: Object Tree > Section List > Standard Section > Position Step Size). This proved useful in examining the compliance of the meshed object to the imaged biology.

Preprints (www.preprints.org) | NOT PEER-REVIEWED | Posted: 10 May 2022 doi:10.20944/preprints202205.0136.v1

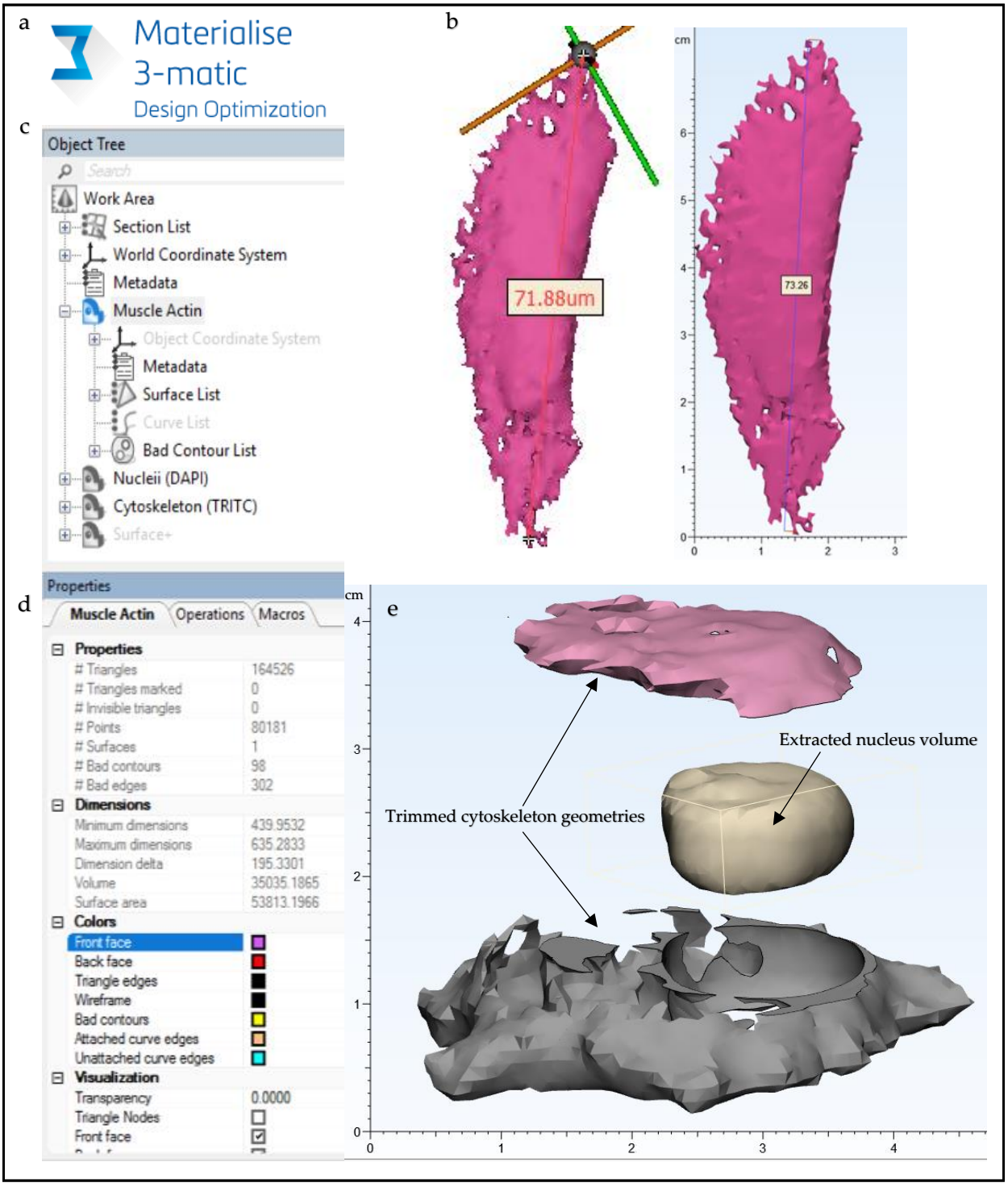


**Figure 3.** Post processing workflow. (a) Materialise 3-Matic software; **(b)** Length and scale verification of HDF Nuclei (DAPI) in Mimics Research (L; um) and 3-Matic Research (R; cm); **(c)** 3-Matic Object Tree displaying imported HDF geometries (α-SMA (Alexa Fluor 647), Nuclei (DAPI), Cytoskeleton (TRITC)) and software metadata; **(d)** a screenshot of the Selected Object Properties tab for a HDF a-SMA muscle actin (Alexa Fluor 647) part in the Materialise 3-Matic user interface; **(e)** Post-processed PANC-1 cell model (cm) designed for greater interactivity. Note the nucleus geometry was Boolean-subtracted from the cytoskeleton with positive clearance factor for post-printing compatibility. The cytoskeleton geometry was also split into upper and lower parts to allow for interactivity.

At this stage, meshes were representative of surfaces only, making them impossible to print with extruded filament of a non-negligible thickness. In practice, printing surfaces with thicknesses greater than or equal to 1 mm generate stable models, although this may vary with printing material and printer used. In *Mimics 3-Matic*, the meshes were uniformly offset (Tool: Design > Uniform Offset > Solid) by a minimum distance of 1 mm,

 doi:10.20944/preprints202205.0136.v1

with the solid fill option checked. Next, the models were smoothed (Tool: Fix > Smooth; or Fix > Reduce; or Fix > Wrap; or Finish > Local Smoothing; or Remesh) to simplify tesselation and hence reduce printing time and cost. This action is also known to improve the likelihood of printing success without sacrificing significant resolution.

To improve the educational interactivity of the models, a range of editing tools in available in the software. In the presented CiTo-3DP methodology, the PANC-1 model was trimmed (Tool: Finish > Trim > Preserve Inner and Outer) to split the cytoskeleton component in two. Further to this, the nucleus component was removed, with a positive clearance factor in mm, from the cytoskeleton, allowing it to fit neatly inside the split parts (Tool: Design > Local Boolean > Subtraction). If components are to be joined together by design slots or joints, a datum plane must be defined (Tool: Design > Create Analytical Primitive > Create Datum Plane), such that the relevant geometry may be cut (Tool: Design > Cut) about the plane and designed for fitting (Tool: Design > Create Primitive; Design > Boolean Union). Note that compliance and compatibility must be carefully considered for part-fitting.

To finalise the meshed geometries, the software automatic mesh corrector algorithm (Tool: Fix > Fix Wizard > Follow Advice) was used. After this, the respective objects, now optimised for 3D printing, are exported as STL files into relevant pre-printing software. In our methodology, these STL files were opened in *Ultimaker's* pre-print software *CURA*.

### *2.6. Printing*

*CURA* is an open access software, allowing users to import STL files into a virtual 3D workplace of the specific printer chosen for printing (Figure 4).

Prior to opening the relevant STL files, *CURA* was configured to the printer used (Tool: Add Printer). A wide range of pre-set printer configurations from *Ultimaker* and other 3D printing companies is included in the software. The size of the printing bed, the type and number of extruders and the material used for extrusion were all defined, as were the slice orientations, layer thickness, infill, and settings for the printing of supports. The software also provided a 3D virtual preview of the print process to visualise the model as it would be printed, allowing further edits and refinements to the print strategy prior to actual printing. The relevant STL models, which use the 3-matic mm-scale, were imported and adjusted to best fit on the printing bed. Any changes to scale were noted.

Since the presented workflow was used as proof-of-concept, the printing configurations were selected for fast PLA printing, which correlates to a printed layer height of 0.2 mm. Notably, printing speed is directly related to layer height in millimetres, and hence determines the quality or resolution of the final print. Shell thickness, or the number of horizontal layers in each shell, affects the final stability of the print, as does infill. A triangular infill of 10% was used for fast printing. Supports were generated, followed by object slicing, which determined the exact printing path the extruder would follow.

The printing configuration and path followed determines the speed of the print and the amount of material used. The sliced objects were exported directly into the printing hardware. Printing was initially observed to check for common 3D printing errors such as extruder clogging or poor build plate adhesion. Once printing was finished, models were allowed to cool, and then removed from the build plate. Printing supports were removed manually. As such, a 3D reconstruction of a complex cell geometry, imaged using confocal microscopy, was printed.

Preprints (www.preprints.org) | NOT PEER-REVIEWED | Posted: 10 May 2022 doi:10.20944/preprints202205.0136.v1

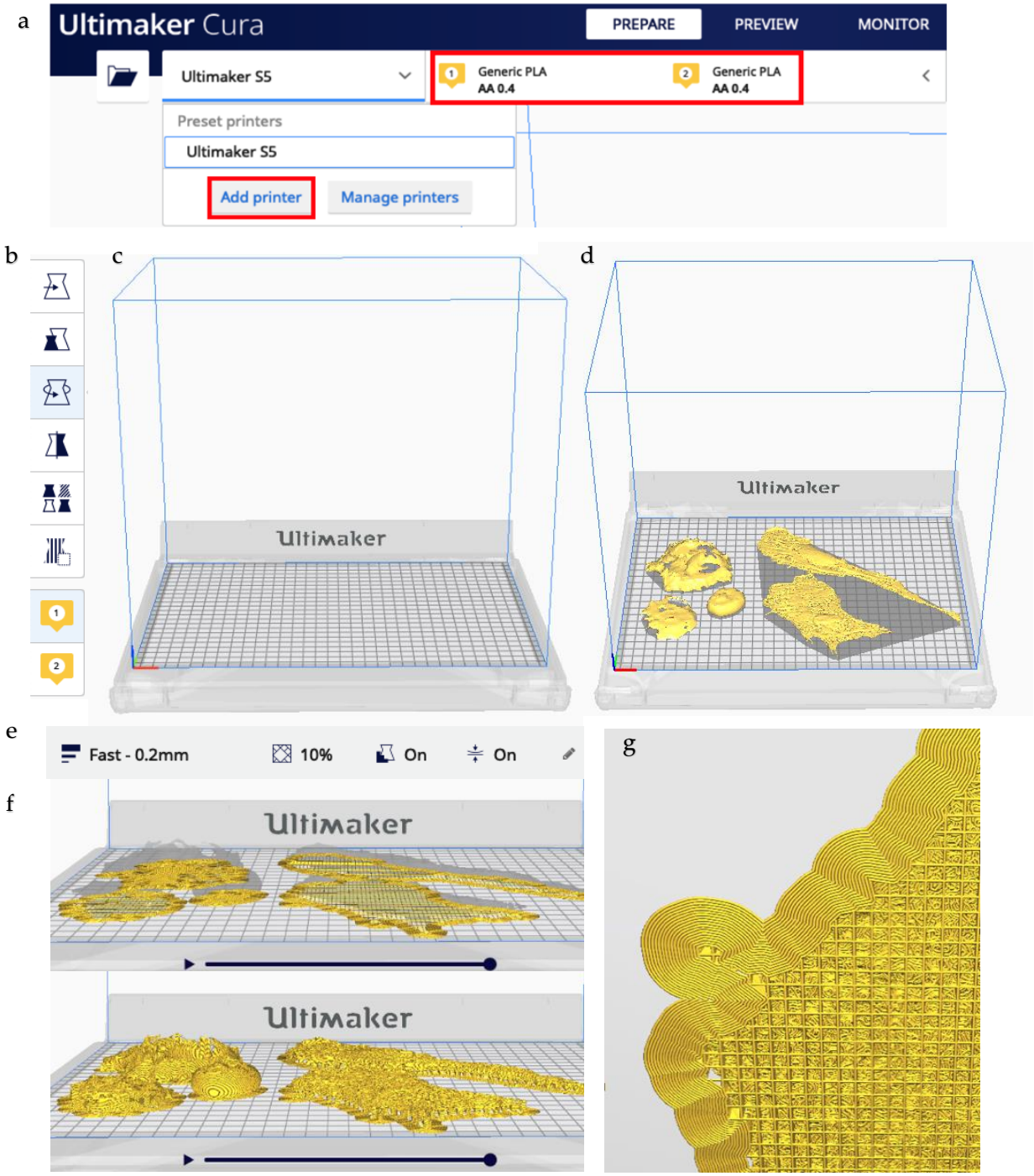


**Figure 4.** The 3D printing procedure. **(a)** Configuring the Ultimaker CURA software. Printer and material configuration tools are highlighted. **(b)** Pre-print editing toolbox. **(c)** Virtual Ultimaker S5 printer. **(d)** PANC-1 and HDF cell .stl files imported into software. **(e)** Print settings. **(f)** Post-slicing virtual printing check. **(g)** Base plate support structures. Note that these are removed after printing.

## 3. Representative results

The following representative results demonstrate the outcomes of the application of the CiTo-3DP methodology described above.

The resolution of each print was calculated using the printing scale and layer height. The results of these calculations are shown in

**Table** 4.

Preprints (www.preprints.org) | NOT PEER-REVIEWED | Posted: 10 May 2022 doi:10.20944/preprints202205.0136.v1

**Table 4.** Printing resolution.

| Parameters | Cell type | |
|---|---|---|
| | PANC-1 | HDF |
| Printing scale, % | 200 | 100 |
| Print scale [um:mm] | 0.5 | 1 |
| Layer height [mm] | 0.2 | 0.2 |
| Resolution [um] | 0.1 | 0.2 |

The resulting 3D printed cellular models of HDF and PANC-1 cells are depicted in Figure 5. The interactive dismountable design of the PANC-1 cells was also verified, as shown in Figure 5 c.

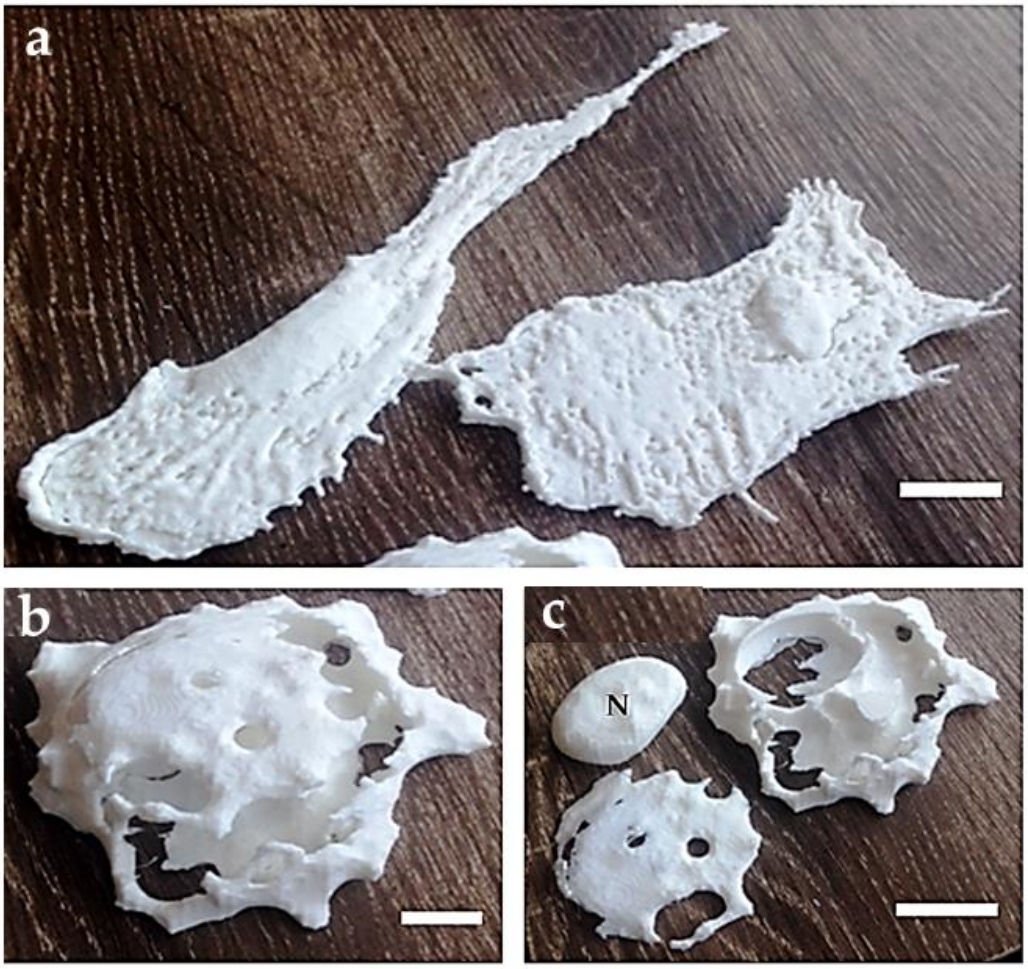


**Figure 5.** Printed PLA models of cells. **(a)** HDF cells. Note the elongated and flattened shape of the cells. Such flattening is typical feature of the cells cultured in vitro in monolayers on a stiff substrate. Scale bar: 2 cm (physical model): 20 μm (cell visualization by scanning confocal microscopy). **(b)** "Enclosed" PANC-1 model. Scale bar: 1 cm (physical model): 10 μm (actual cell dimensions observed by scanning confocal microscopy). **(c)** Dismountable PANC-1 cell model in the "open" state - with nucleus (N) removed from the two parts representing the surrounding f-actin cytoskeleton. The "niche" formed by the cytoskeleton f-actin filaments that surrounds the nucleus in the cell is clearly visible in the top right fragment. Scale bars indicate the original dimensions of the cells. Scale bar: 2 cm (3D printed model): 20 μm (actual cell dimensions observed by scanning confocal microscopy).

 doi:10.20944/preprints202205.0136.v1

## 4. Discussion

Microscopy-to-3D printing concept allows to up-scale the unseen world of microscopy into the perceptible matter. Further to this, it provides researchers and educators with a tool to present their discoveries and teaching content at a more comprehensible scale, making it easier to communicate on the complex subjects.

In the current study, FDM printing technology was used to produce CAD-generated 3D reconstructions of confocal microscopy whole-cell imaging data.

We utilized FDM 3D printing in our CiTo-3DP methodology due to its ease of use, speed, considerable commercial availability and affordable operation. The FDM technology has reasonable resolution capabilities, with most commercial products able to print to actual resolutions, or extrusion layer-heights, of down to 100 µm [15]. FDM 3D printing devices are also capable of printing other materials with varying physical attributes, such as flexibility, strength and transparency, and colours, although safety and printer compatibility need to be considered. Although we used only white PLA material, the multicoloured and transparent materials with varying flexibilities can be adapted to our proposed CiTo-3DP protocol on the basis of published prototypes [15,21,22]. A virtual 3D model depicting the spatial distribution of f-actin, $\alpha$-SMA and nucleus in a healthy human dermal fibroblast is shown in Figure A1 (Appendix A3). Additional finishing of the models for perception enhancement can be performed, for example, by coating with silicone rubber as shown elsewhere [10].

In our CiTo-3DP workflow, an Ultimaker 3D printer was chosen for model production. The advantage of using Ultimaker hardware is its ease of use, commercial availability, affordability and compatibility with pre-print software CURA. The latter included a virtual 3D visualisation of the print process itself, allowing prior adjustment of various print settings such as print slice orientation, infills and printing of supports. For more complex geometries however, greater control and editing of the printing path could be an advantage in specific cases, although CURA has the advantage of being readily available. In saying that, due to the competitive market, we regarded other 3D printing hardware and software as comparable and easily interchangeable with the presented workflow.

It should be noted that more complex AM-technologies like SLS and Two-Photon 3D Printing are indeed becoming more readily available. These advanced technologies offer greater resolution and precision, potentially making them better-suited to the field of microscopy, where model up-scaling, image resolution and printing accuracy are vitally important. However, they appear less accessible and more expensive to entry-level users when compared with FDM 3D printing, and hence will likely experience less uptake into new industries. This would need to be considered if the proposed methodology was to be expanded into higher levels of image magnification using high-resolution microscopy technologies, such as electron microscopy or super-resolution microscopy. For "proof-of-concept" studies, however, our results demonstrate that FDM is sufficient.

The future of image-processing and AM utilization in cell biology and related disciplines is promising. Various steps have been taken towards integrating image-based model simulations into common practice. Togni et al. [46] showed the efficacy of using finite-element method (FEM) multi-physics modelling software in undergraduate biology education, whilst Tang et al. [47] compared the biomechanical heterogeneity of living cells as measured by atomic force microscopy and finite-element simulation. Notably, both used generic computer-defined geometries. To implement this into a 3D printing workflow, further steps would be required to better define the objects. Inspecting surface mesh quality, generating a volume mesh and validating against the imaged biology, would be required as a minimum to ensure accurate modelling. A range of finite element method (FEM) and Computational Fluid Dynamics (CFD) software, such as ANSYS, COMSOL Multiphysics, or even Materialise, are available, providing the file types and sizes that are transferable between software.

Another promising technology entering this field is virtual reality. Virtual reality visualizations require similar image-processing analysis and hence provide equivalent educational benefits to students, all whilst negating the need and hence cost of 3D printing.

 doi:10.20944/preprints202205.0136.v1

This too, has seen limited uptake in cell-biology education. In the study by Cali et al. [45], virtual reality was used to visualize and aid quantitative analysis of reconstructed glial and neuronal cells.

FDM 3D printed cellular and subcellular models has the potential to be used both as a visual aid, as described, and as a quantitative tool. This is of particular interest in the fields of bioengineering, computational biology, cellular and tissue morphometrics, and developmental biology. Analysis of morphogenetic behaviour of living tissues has to-date proven instrumental in biology-related fields [48], and 3D image reconstruction and FDM-printing pose as additional analytical tools. In the presented methodology, the clear differences between the PANC-1 and HDF models were shown across several cellular structures. Image-processing and reconstruction of 3D geometries makes basic morphometric measurements, such as cellular diameter, shape, height and surface area easier to acquire. Additionally, segmentation of various cellular structures allows intra-cellular comparisons to be made. FDM-printing models with the same material would also provide the data on cellular volumetrics. That is, the amount of material required to print cellular structures of different cell types could be used as a comparative measurement. To improve image quality, finer voxel dimensions are recommended. Clearly, the presented workflow could be utilized for quantitative morphometrics with minimal adjustments.

Finally, introducing 3D models for the presentation of experimental results in biological systems is a part of the trend to put discoveries in more translatable models. This is especially instrumental for research conducted on cellular and tissue levels, since both cell microscopy and pathology lose the volumetric perspective. We hope that additive technology models can contribute to better understanding of the spatial profile of tissues, accelerating research in the matrix biology and mechanotransduction.

The development of this approach has the potential to further revolutionize science education, by providing a strong nexus between laboratory skills, computational analysis and communication of results [15]. This method has already been utilized in advancing the analysis of biomolecular data sets in the teaching of complex chemical molecular structures [21]. It is reasonable to suggest that AM technology applied for the reconstruction of micron-scale biological objects can contribute to knowledge generation advancement in life and material sciences, engineering and medicine.

It should be noted that 3D printing does not come without limitations. Firstly, and most importantly, model quality is intrinsically dependent on microscopy image quality. That is, the mode of image acquisition has a direct impact on the final quality of results. Available computational power should also be considered in regard to any increase in imaging resolution. Furthermore, using our proposed CiTo-3DP methodology, it is difficult to visualize smaller cellular structures, such as ribosomes, even after up-scaling. Beyond the image quality and microscope resolution, it is also constrained by the resolution capacity of FDM-printing and the spatial limitations of commercial printers. That is, increasing scaling factors to visualize more detailed biological structures would hinder project time, cost, and model ease-of-interactivity. As previously discussed, other forms of AM-technology with higher precision could be utilized to effectively see further into the cell. Finally, designing highly complex cellular visualizations to be interactive can be difficult, with some structures and cell-types being more suitable than others.

Nevertheless, the CiTo-3DP methodology we have outlined is highly transferrable and flexible. Here, we have merely provided an example of its use, without fully describing its potential in different fields of research and education.

In conclusion, the presented CiTo-3DP methodology contributes to bringing of the reach of AM further into the biological sciences, providing researchers and educators with a new to display and analyze complex biological data. We envisage that the resulting CAD and 3D printed models could be used for further applications, including but not limited to in silico simulations for biology, medicine, pharmacological research, tissue engineering, morphometrical analysis, multiphysics modelling, education, rehabilitation of visually impaired people, and integration into virtual reality.

**Author Contributions:** Conceptualization, X.F. and A.G.; methodology, X.F., A.F., S.D. and A.G.; software, X.F. and S.D.; validation, X.F. and A.F.; formal analysis, X.F.; investigation, X.F.; resources, S.D. and A.G..; data curation, X.F. and A.F.; writing—original draft preparation, X.F.; writing—review and editing, X.F., A.F., S.D. and A.G.; visualization, X.F. and A.F.; supervision, S.D. and A.G.; project administration, A.G.; funding acquisition, A.G. All authors have read and agreed to the published version of the manuscript.

**Funding:** This study was supported by the Taste of Research Scholarship to X. F. provided by The Graduate School of Biomedical Engineering, UNSW. The work of A.F. was supported by the Ministry of Science and Higher education of Russian Federation within the framework of state support for the creation and development of World-Class Research Center "Digital biodesign and personalized healthcare", grant number NO. 075-15-2020-926.

**Institutional Review Board Statement:** Not applicable.

**Informed Consent Statement:** Not applicable.

**Data Availability Statement:** The relevant data generated and used in the current study is available from the corresponding author upon reasonable request.

**Acknowledgments:** X.F. A.F. and A.G. thank to Prof Ewa Goldys (UNSW) for her devoted mentorship support and helpful discussions. Authors thank Dr Sandhya Clement (UNSW and University of Sydney) for providing PANC-1 cells. X.F. thank to the team at the Digital Fabrication Lab (3D Printing) facility (https://www.making.unsw.edu.au/dfl/facilities/digital-fabrication-lab-3d-printing/) for the help in development of the 3D printing protocol. X.F., A.F., and A.G. thank Dr Ayad Anwer and Dr Lynn Ferris (UNSW) for the laboratory operations support. Additional thanks to the team at the UNSW Digital Fabrication Lab (3D Printing) facility for their support in printing.

**Conflicts of Interest:** The authors declare no conflict of interest. The funders had no role in the design of the study; in the collection, analyses, or interpretation of data; in the writing of the manuscript, or in the decision to publish the results.

## Appendix A

### *A1. The Biomedical Educational and Research Context*

The link between education and AM has previously been made by Kaplan et al. [20] and others, showing learning outcomes of complex concepts are greatly improved through the production of physical data visualizations. Further to this, education is made more accessible and comprehensible to special needs and disabled students. Similar conclusions have been drawn in cell-biology and microscopy-related fields by Perry et al. [6]. In these fields, image data is often visualized 3-dimensionally in silico, on analytically powerful software like ImageJ [45]. Visualizing data in this way is effective but requires additional cognitive load to isometrically decode within the human brain. 3D printing data reconstructions effectively reduces this cognitive load, and as such, has the capacity to revolutionize how scientists analyze and present their results and findings.

In biomedical and bioengineering education, the presented CiTo-3DP methodology may be used to improve learning outcomes associated with complex biological concepts, such as cell morphology and tissue development. Additive technologies can provide biological constructors consisting of cellular and subcellular parts which can become a great way to teach spatial concepts such as tissue architecture and intracellular compartmentalization.

The CiTo-3DP method goes beyond the teaching of "generic" eukaryotic cell types by showing the obvious variety in cell morphometry between PANC-1 and HDF cells (Figure 5). As an example, students could be led through a laboratory-based experiment to culture and image basic mammalian cell phenotypes from epithelial, mesenchymal or endodermal tissue origin. Other complex concepts such as cancer pathogenesis, cell shape regulation, EMT/MET, fibrosis, cell phenotypes and transdifferentiation, as well as the general concept of dimensionalities - can be explored in specially designed experiments that now can be enhanced with 3D tactile visualization.

Students could then develop their own interactive models in image-processing-compatible CAD software and 3D print them using FDM printers located at their respective

Preprints (www.preprints.org) | NOT PEER-REVIEWED | Posted: 10 May 2022 doi:10.20944/preprints202205.0136.v1

institutes. Such a workflow would provide students with hands-on experience in cell culturing, microscopy imaging, computational data analysis and CAD, whilst also providing them with enhanced learning outcomes.

We suggest that some aspects of the presented CiTo-3DP protocols are particularly relevant for the biological and biomedical educational and research context.

- Cell culture terminology and methodology: linear (immortalized) cells vs primary cells [26]. The technical article by Merck explains cell culture protocols applicable both to linear cells (presented by cancer PANC-1 cells) and primary cells (human dermal fibroblasts, HDF).
- Healthy cells (HDF) vs cancer cells (PANC-1). Fibroblasts are the main cell type in connective tissues, responsible for the production and degradation of collagen and other components of extracellular matrix. A specialized form of fibroblasts, myofibroblasts, can exert strong contraction of tissue (particularly important for wound healing and regeneration). The source of PANC-1 cells is the pancreatic ductal adenocarcinoma, a deadly cancer with limited treatment options [27,28]. This malignant tumor commonly contains large amounts of collagen and fibroblasts, which together contribute to its treatment resistance [29].
- Embryonic origin of cells and tissues. Pancreatic adenocarcinoma originates from pancreatic glandular epithelium which has ectodermal embryonic origin. Fibroblasts are the cells of mesodermal origin.
- Cell shape and phenotype. Untreated PANC-1 cells are characterized by epithelioid phenotype; the HDFs have a mesenchymal-like phenotype. Among several classifying features, morphology is one of the most prominent and obvious signatures of cellular phenotype. Epithelioid cells have a rounded shape, and their nucleus is usually centrally located. The signature of mesenchymal cells is a more elongated shape, quite often spindle-like, and the nucleus of the cell is usually more eccentric [26]. Cell shape is a recognized feature associated with adhesion and motility potential, as well as their differentiation commitment [30-32].
- EMT and MET. One of the critical hallmarks of cancer progression is the so-called epithelial-to-mesenchymal transition (EMT) and the reverse (MET) process, reflecting the adaptation of cancer cells to new environments, for example, during the metastatic colonization of distant organs. The signature for EMT is a loss of epithelioid phenotype in epithelial (healthy or malignant) cells, and the acquisition of a mesenchymal phenotype. MET presents the opposite transition. EMT/MET phenotype changes are reflected, in particular, in cell shape [33,34].
- Fibrosis. Fibrosis is the scarring of tissues and organs, characterized by excessive accumulation of extracellular matrix. At certain stages, it is also associated with rapid proliferation of fibroblasts and their transformation into myofibroblasts. The signature of myofibroblasts is expression of $\alpha$-Smooth Muscle Actin ($\alpha$-SMA). The fibroblast-to-myofibroblast transdifferentiation, as well as transformation of other cells into myofibroblasts, is a typical sign of fibrosis [35-39].
- Cytoskeleton. Three types of subcellular structures were imaged in the current study: cell nuclei, polymerised f-actin filaments representing the cytoskeleton component defining the shape of cells [30-32], and the specialized form of actin, known as $\alpha$-smooth muscle actin ($\alpha$-SMA), which is recognized as a phenotypical marker of cells bearing mechanical stress, such as smooth muscle cells or myofibroblasts [40]. Both the shape of the cytoskeleton and the level of $\alpha$-SMA expression are key indicators of cell functional state. Cell cytoskeleton and nucleus shape are dynamic characteristics that can reflect the phase of the mitotic cycle and the migration pattern [41]. In standard two-dimensional cell culture models, larger mean surface area and proportion of

Preprints (www.preprints.org) | NOT PEER-REVIEWED | Posted: 10 May 2022 doi:10.20944/preprints202205.0136.v1

contractile $\alpha$-SMA fibers indicate myofibroblast transdifferentiation of fibroblasts followed by excess synthesis of collagen [42]. This phenotypical transition reflects cellular fibrotic response on the tissue level, e.g., in skin scar or peri-implant connective tissue capsule formation [43]. These parameters are important to monitor in in vitro studies of cancer treatment, drug testing and in all the areas where cells are responding to external factors.

- The research and bioengineering applications of the CiTo-3DP methodology are dependent on the choice of the cells and subcellular structures. For the printed cellular models presented in this study, we envisage a scope of analytical tasks related to the relationship between the nucleus and cytoskeleton. For example, the data on the mass vs the volume of the organelles, the surface texture of the organelles, the architecture of the intracellular space, and their reorganization in response to the experimental stimuli could serve for more biologically accurate bioengineering simulations such as, for instance, computational fluid dynamics research and analysis of the intracellular mechanical microenvironment. Further development of the proposed approach with the development of multimaterial models or layered multimaterial coatings, may be useful in cognitive and rehabilitation sciences.

*A2. Technical notes*

- In the proposed workflow, 2D confocal microscopy image z-stacks were spliced together using GV-intensity thresholding in Mimics Research 21.0 software. PANC-1 and HDF cells were separately cultured and stained for immunofluorescent visualization of nuclei and cytoskeletal structures under a confocal laser scanning microscope. Respective .tiff z-stack files and corresponding image .txt metadata files were created as follows: 16 PANC-1 culture XY-planar images were sequentially captured and stacked under 60X oil-submerged magnification, generating an XYZ voxel resolution of 0.207 × 0.207 × 1.000 [μm/pixel3]. Similarly, 33 HDF culture XY-planar images were sequentially captured and stacked under 20× magnification, generating an XYZ voxel resolution of with XYZ voxel resolution of 0.621 × 0.621 × 0.500 [μm/pixel3]. Both sets of images were optimised by adjusting laser intensity and voltage gain and offset of the PMT-amplified signal.
- Note that voxel resolution was identified as the principal determinant of image quality and hence 3D reconstruction accuracy.
- The open-source Ultimaker software CURA was used to prepare the .stl files for 3D printing and configure the print settings of the selected printer. Both cell types were printed simultaneously on a dual-extrusion Ultimaker S5 FFF-technology printer with a 330 x 240 x 300 mm build volume.
- White PLA material was extruded at 205°C through a 0.4 mm extruder head onto a build plate surface at 65°C. Fast printing settings were chosen to minimise printing time, which came to approximately 12 hours. In particular, a 10% infill and 60° support angle were chosen. The printer was allowed to cool prior to removing the printed models from the build plate. Supports were removed by hand and with the aid of plyers.
- Cropped 3D reconstructions of cellular structures were generated in Mimics Research 21.0 software from the imported z-stacks using grey-value thresholding. A single PANC-1 cell and two connected HDF cells were respectively isolated. Minor edits were made to masks to better represent the cellular components imaged. Specifically, the Smart Fill tool was used to fill small holes between reconstructed voxels.
- This was particularly important in generating close-to solid nucleus structures. An initial length measurement of a selected nucleus object was taken in μm for scale verification throughout the workflow. The resultant objects were exported directly into Mimics 3-Matic for post-processing. A second

 doi:10.20944/preprints202205.0136.v1

length measurement of the previously selected nucleus object was taken in mm, which verified the import rescaling from μm to mm automatically performed by the Mimics software.

- The 3D objects were optimized for 3D printing using various editing tools. A 1mm external uniform offset was applied to the meshed surface geometries, followed by iterations of the smoothing, wrapping and remeshing tools. The PANC-1 model was designed such that the nucleus could be extracted from the rest of the model. To achieve this, an XY-plane trim was performed to slice the cytoskeleton geometry in half. The aligned nucleus geometry was then Boolean-subtracted with a 1 mm clearance factor from the trimmed cytoskeleton geometries.
- Finally, the quality of the resultant surface meshes were checked using the Fix Wizard tool. Three PANC-1 surfaces (nucleus, cytoskeleton upper, cytoskeleton lower) and a single HDF surface were exported as separate .stl files.Mimics and 3-Matic (Materialise) are already readily used in Biomedical research applications as a design-orientated software.
- As previously noted, Mimics has been used by Liu et al. [16] to improve surgical planning and performance, as well as by McMenamin et al. [15] as a cheaper and more ethically neutral alternative teaching aid to cadavers in medical education. In comparison to other commercial software, Martin et al. [9] showed that Mimics possessed more powerful image manipulation, visualization and editing functions. 3-matic, also part of Materialise and often packaged with Mimics, allows for further design iterations and is well-suited to optimizing meshes for FDM 3D printing as STL files.
- Notably, neither software has seen significant uptake in areas of micro-scale biology. In comparison to open-access image-processing software such as 3D Slicer and ImageJ, commercial software provides a faster, more powerful and more versatile user experience. In terms of CAD, commercial software, like 3-Matic, allows for greater interactivity to be easily built into printable models. Although this design-power was not fully explored in this methodology, its effect was demonstrated by the interactivity of the PANC-1 cytoskeleton-nucleus cell model. To achieve similar results using free software would require transfer between software, which is often cumbersome in terms of file-formatting and file sizes. Considering that Materialise provides both image-processing and CAD, and is already used in biology-related sciences, it was chosen for this project. It should be noted that Materialise also offers a variety of online tutorial resources, making it far easier to learn the software.

*A3. 3D reconstruction of human dermal fibroblasts with differentially stained subcellular components*

 doi:10.20944/preprints202205.0136.v1

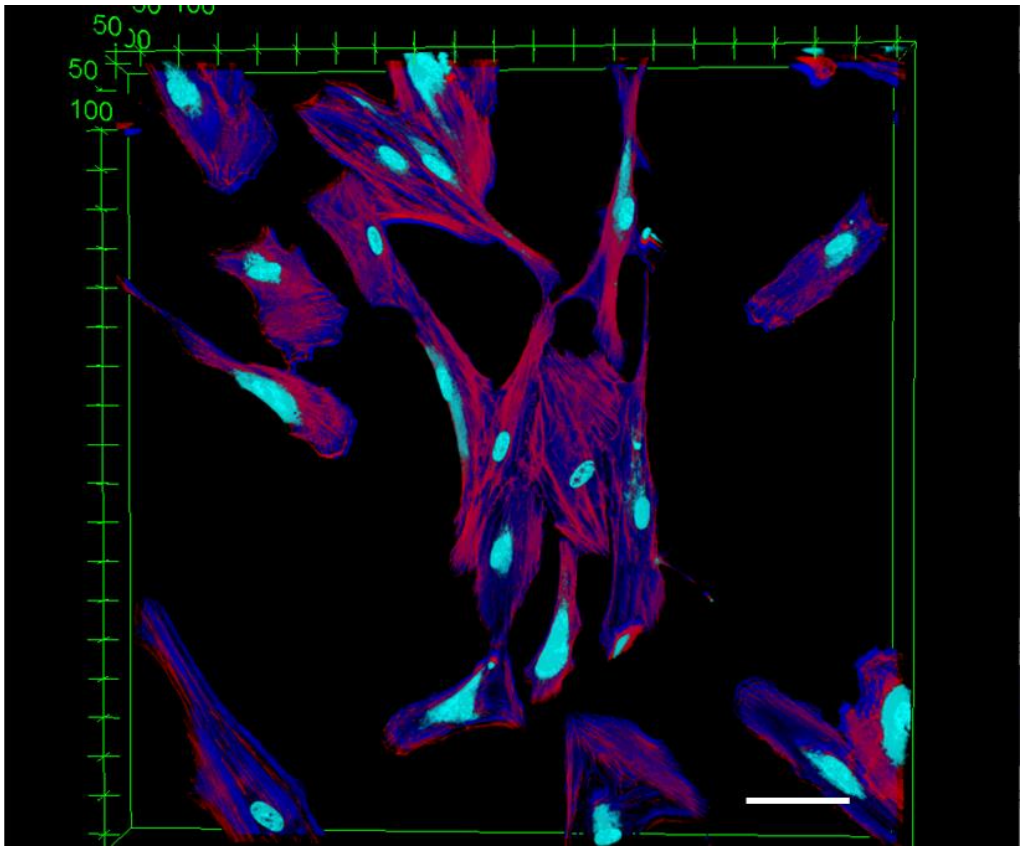


**Figure A1.** Virtual multicoloured (false-palleted) 3D model of healthy human dermal fibroblasts cultured in a monolayer on cell culture plastic substrate. Note differentially stained subcellular structures: centrally positioned ellipsoid and elongated nuclei (turquoise, DAPI), α-SMA actin fibers that surround the nuclei (blue, secondary antibody conjugated with Alexa Fluor 647), and the f-actin stress fibers located at the cortical surfaces of the cells (red, phalloidin-TRITC). Reconstruction from a confocal microscopy z-stack, containing 99 individual slices for each fluorophore channel using FiJi (ImageJ) 3D Viewer plugin. Scale bar: 100 μm.

## References

1. Ngo, T.D.; Kashani, A.; Imbalzano, G.; Nguyen, K.T.Q.; Hui, D. Additive manufacturing (3D printing): A review of materials, methods, applications and challenges. *Compos Part B-Eng* **2018**, *143*, 172-196, doi:10.1016/j.compositesb.2018.02.012.
2. Ahangar, P.; Cooke, M.E.; Weber, M.H.; Rosenzweig, D.H. Current Biomedical Applications of 3D Printing and Additive Manufacturing. *Appl Sci-Basel* **2019**, *9*, 1713, doi:ARTN 1713 10.3390/app9081713.
3. Calignano, F.; Galati, M.; Iuliano, L.; Minetola, P. Design of Additively Manufactured Structures for Biomedical Applications: A Review of the Additive Manufacturing Processes Applied to the Biomedical Sector. *J Healthc Eng* **2019**, *2019*, 9748212, doi:10.1155/2019/9748212.
4. Attaran, M. The rise of 3-D printing: The advantages of additive manufacturing over traditional manufacturing. *Business Horizons* **2017**, *60*, 677-688, doi:10.1016/j.bushor.2017.05.011.
5. Mace, E.M.; Moon, J.; Orange, J.S. Three-Dimensional Printing of Super-Resolution Microscopy Images. *Microscopy Today* **2015**, *23*, 26-29, doi:10.1017/s1551929515000607.
6. Perry, I.; Szeto, J.-Y.; M D, I.; E C, G.; R, R.; Scofield, S.; P D, W.; Hayes, A. Production of 3D Printed Scale Models from Microscope Volume Datasets for use in STEM Education. *EMS Engineering Science Journal* **2017**, *1*.
7. Del Rosario, M.; Heil, H.; Mendes, A.; Saggiomo, V.; Henriques, R. The Field Guide to 3D Printing in Microscopy. *Preprints* **2021**, *2021050352*, doi:10.20944/preprints202105.0352.v1.

8. Baghaie, A.; Pahlavan Tafti, A.; Owen, H.A.; D'Souza, R.M.; Yu, Z. Three-dimensional reconstruction of highly complex microscopic samples using scanning electron microscopy and optical flow estimation. *PloS one* **2017**, *12*, e0175078, doi:10.1371/journal.pone.0175078.
9. Martin, C.M.; Roach, V.A.; Nguyen, N.; Rice, C.L.; Wilson, T.D. Comparison of 3D reconstructive technologies used for morphometric research and the translation of knowledge using a decision matrix. *Anat Sci Educ* **2013**, *6*, 393-403, doi:10.1002/ase.1367.
10. Werz, S.M.; Zeichner, S.J.; Berg, B.I.; Zeilhofer, H.F.; Thieringer, F. 3D Printed Surgical Simulation Models as educational tool by maxillofacial surgeons. *Eur J Dent Educ* **2018**, *22*, e500-e505, doi:10.1111/eje.12332.
11. Wojtyla, S.; Klama, P.; Baran, T. Is 3D printing safe? Analysis of the thermal treatment of thermoplastics: ABS, PLA, PET, and nylon. *J Occup Environ Hyg* **2017**, *14*, D80-D85, doi:10.1080/15459624.2017.1285489.
12. Tack, P.; Victor, J.; Gemmel, P.; Annemans, L. 3D-printing techniques in a medical setting: a systematic literature review. *Biomedical engineering online* **2016**, *15*, 115, doi:10.1186/s12938-016-0236-4.
13. Manero, A.; Smith, P.; Sparkman, J.; Dombrowski, M.; Courbin, D.; Kester, A.; Womack, I.; Chi, A. Implementation of 3D Printing Technology in the Field of Prosthetics: Past, Present, and Future. *Int J Environ Res Public Health* **2019**, *16*, doi:10.3390/ijerph16091641.
14. Zadpoor, A.A.; Malda, J. *Additive manufacturing of biomaterials, tissues, and organs*; Springer: 2017.
15. McMenamin, P.G.; Quayle, M.R.; McHenry, C.R.; Adams, J.W. The production of anatomical teaching resources using three-dimensional (3D) printing technology. *Anat Sci Educ* **2014**, *7*, 479-486, doi:10.1002/ase.1475.
16. Liu, P.; Hu, Z.; Huang, S.; Wang, P.; Dong, Y.; Cheng, P.; Xu, H.; Tang, B.; Zhu, J. Application of 3D Printed Models of Complex Hypertrophic Scars for Preoperative Evaluation and Surgical Planning. *Front Bioeng Biotechnol* **2020**, *8*, 115, doi:10.3389/fbioe.2020.00115.
17. Bernhard, J.C.; Isotani, S.; Matsugasumi, T.; Duddalwar, V.; Hung, A.J.; Suer, E.; Baco, E.; Satkunasivam, R.; Djaladat, H.; Metcalfe, C.; et al. Personalized 3D printed model of kidney and tumor anatomy: a useful tool for patient education. *World J Urol* **2016**, *34*, 337-345, doi:10.1007/s00345-015-1632-2.
18. Witowski, J.S.; Pedziwiatr, M.; Major, P.; Budzynski, A. Cost-effective, personalized, 3D-printed liver model for preoperative planning before laparoscopic liver hemihepatectomy for colorectal cancer metastases. *Int J Comput Assist Radiol Surg* **2017**, *12*, 2047-2054, doi:10.1007/s11548-017-1527-3.
19. Hachulla, A.L.; Noble, S.; Guglielmi, G.; Agulleiro, D.; Muller, H.; Vallee, J.P. 3D-printed heart model to guide LAA closure: useful in clinical practice? *Eur Radiol* **2019**, *29*, 251-258, doi:10.1007/s00330-018-5569-x.
20. Kaplan, H.; Pyayt, A. Tactile visualization and 3D printing for education. *Encyclopedia of Computer Graphics and Games* **2015**, 1-8, doi:10.1007/978-3-319-08234-9_57-1.
21. Da Veiga Beltrame, E.; Tyrwhitt-Drake, J.; Roy, I.; Shalaby, R.; Suckale, J.; Pomeranz Krummel, D. 3D Printing of Biomolecular Models for Research and Pedagogy. *Journal of visualized experiments : JoVE* **2017**, e55427, doi:10.3791/55427.
22. Cox, B.L.; Schumacher, N.; Konieczny, J.; Reifschneider, I.; Mackie, T.R.; Otegui, M.S.; Eliceiri, K.W. Fabrication approaches for the creation of physical models from microscopy data. *3D Print Med* **2017**, *3*, 2, doi:10.1186/s41205-017-0011-6.
23. Augusto, I.; Monteiro, D.; Girard-Dias, W.; Dos Santos, T.O.; Rosa Belmonte, S.L.; Pinto de Oliveira, J.; Mauad, H.; da Silva Pacheco, M.; Lenz, D.; Stefanon Bittencourt, A.; et al. Virtual Reconstruction and Three-Dimensional Printing of Blood Cells as a Tool in Cell Biology Education. *PloS one* **2016**, *11*, e0161184, doi:10.1371/journal.pone.0161184.
24. Holt, K.; Savoian, M. Epi-fluorescence microscopy and 3D printing: An easily implemented approach for producing accurate physical models of micro-and macro-scopic biological samples. In *Microscopy and imaging*

*science: practical approaches to applied research and education*, Méndez-Vilas, A., Ed.; Formatex Research Centre: Badajoz, Spain, 2017; pp. 697-702.

25. Mai, K.K.K.; Kang, M.J.; Kang, B.-H. 3D Printing of Plant Golgi Stacks from Their Electron Tomographic Models. In *Plant Protein Secretion: Methods and Protocols*, Jiang, L., Ed.; Springer New York: New York, NY, 2017; pp. 105-113.
26. Merck. Cell Types & Culture Characteristics. Available online: https://www.sigmaaldrich.com/AU/en/technical-documents/technical-article/cell-culture-and-cell-culture-analysis/mammalian-cell-culture/cell-types-culture (accessed on 21.12.2021).
27. Garrido-Laguna, I.; Hidalgo, M. Pancreatic cancer: from state-of-the-art treatments to promising novel therapies. *Nat Rev Clin Oncol* **2015**, *12*, 319-334, doi:10.1038/nrclinonc.2015.53.
28. Raimondi, S.; Maisonneuve, P.; Lowenfels, A.B. Epidemiology of pancreatic cancer: an overview. *Nature reviews. Gastroenterology & hepatology* **2009**, *6*, 699-708, doi:10.1038/nrgastro.2009.177.
29. Awaji, M.; Futakuchi, M.; Heavican, T.; Iqbal, J.; Singh, R.K. Cancer-Associated Fibroblasts Enhance Survival and Progression of the Aggressive Pancreatic Tumor Via FGF-2 and CXCL8. *Cancer microenvironment : official journal of the International Cancer Microenvironment Society* **2019**, *12*, 37-46, doi:10.1007/s12307-019-00223-3.
30. Mendez, M.G.; Kojima, S.; Goldman, R.D. Vimentin induces changes in cell shape, motility, and adhesion during the epithelial to mesenchymal transition. *FASEB journal : official publication of the Federation of American Societies for Experimental Biology* **2010**, *24*, 1838-1851, doi:10.1096/fj.09-151639.
31. McBeath, R.; Pirone, D.M.; Nelson, C.M.; Bhadriraju, K.; Chen, C.S. Cell shape, cytoskeletal tension, and RhoA regulate stem cell lineage commitment. *Developmental cell* **2004**, *6*, 483-495, doi:10.1016/s1534-5807(04)00075-9.
32. Lecuit, T.; Lenne, P.F. Cell surface mechanics and the control of cell shape, tissue patterns and morphogenesis. *Nat Rev Mol Cell Biol* **2007**, *8*, 633-644, doi:10.1038/nrm2222.
33. Rozova, V.S.; Anwer, A.G.; Guller, A.E.; Es, H.A.; Khabir, Z.; Sokolova, A.I.; Gavrilov, M.U.; Goldys, E.M.; Warkiani, M.E.; Thiery, J.P.; et al. Machine learning reveals mesenchymal breast carcinoma cell adaptation in response to matrix stiffness. *PLoS Comput Biol* **2021**, *17*, e1009193, doi:10.1371/journal.pcbi.1009193.
34. Antony, J.; Thiery, J.P.; Huang, R.Y. Epithelial-to-mesenchymal transition: lessons from development, insights into cancer and the potential of EMT-subtype based therapeutic intervention. *Physical biology* **2019**, *16*, 041004, doi:10.1088/1478-3975/ab157a.
35. Schulz, J.N.; Plomann, M.; Sengle, G.; Gullberg, D.; Krieg, T.; Eckes, B. New developments on skin fibrosis - Essential signals emanating from the extracellular matrix for the control of myofibroblasts. *Matrix biology : journal of the International Society for Matrix Biology* **2018**, *68-69*, 522-532, doi:10.1016/j.matbio.2018.01.025.
36. Pakshir, P.; Hinz, B. The big five in fibrosis: Macrophages, myofibroblasts, matrix, mechanics, and miscommunication. *Matrix biology : journal of the International Society for Matrix Biology* **2018**, *68-69*, 81-93, doi:10.1016/j.matbio.2018.01.019.
37. Bochaton-Piallat, M.L.; Gabbiani, G.; Hinz, B. The myofibroblast in wound healing and fibrosis: answered and unanswered questions. *F1000Res* **2016**, *5*, F1000 Faculty Rev-1752, doi:10.12688/f1000research.8190.1.
38. Willis, B.C.; duBois, R.M.; Borok, Z. Epithelial origin of myofibroblasts during fibrosis in the lung. *Proc Am Thorac Soc* **2006**, *3*, 377-382, doi:10.1513/pats.200601-004TK.
39. Radisky, D.C.; Kenny, P.A.; Bissell, M.J. Fibrosis and cancer: do myofibroblasts come also from epithelial cells via EMT? *J Cell Biochem* **2007**, *101*, 830-839, doi:10.1002/jcb.21186.
40. Jones, C.; Ehrlich, H.P. Fibroblast expression of alpha-smooth muscle actin, alpha2beta1 integrin and alphavbeta3 integrin: influence of surface rigidity. *Exp Mol Pathol* **2011**, *91*, 394-399, doi:10.1016/j.yexmp.2011.04.007.

41. Fletcher, D.A.; Mullins, R.D. Cell mechanics and the cytoskeleton. *Nature* **2010**, *463*, 485-492, doi:10.1038/nature08908.
42. Shinde, A.V.; Humeres, C.; Frangogiannis, N.G. The role of alpha-smooth muscle actin in fibroblast-mediated matrix contraction and remodeling. *Biochim Biophys Acta Mol Basis Dis* **2017**, *1863*, 298-309, doi:10.1016/j.bbadis.2016.11.006.
43. Fayzullin, A.; Churbanov, S.; Ignatieva, N.; Zakharkina, O.; Tokarev, M.; Mudryak, D.; Khristidis, Y.; Balyasin, M.; Kurkov, A.; Golubeva, E.N.; et al. Local Delivery of Pirfenidone by PLA Implants Modifies Foreign Body Reaction and Prevents Fibrosis. *Biomedicines* **2021**, *9*, 853, doi:10.3390/biomedicines9080853.
44. Merck. Human Dermal Fibroblasts (HDF) Culture Protocol. Available online: https://www.sigmaaldrich.com/AU/en/technical-documents/protocol/cell-culture-and-cell-culture-analysis/primary-cell-culture/human-dermal-fibroblasts (accessed on 15 December 2021).
45. Cali, C.; Kare, K.; Agus, M.; Veloz Castillo, M.F.; Boges, D.; Hadwiger, M.; Magistretti, P. A Method for 3D Reconstruction and Virtual Reality Analysis of Glial and Neuronal Cells. *Journal of visualized experiments : JoVE* **2019**, doi:10.3791/59444.
46. Togni, P.; Cifra, M.; Drizdal, T. COMSOL Multiphysics in Undergraduate Education of Electromagnetic Field Biological Interactions. *14th Nordic-Baltic Conference on Biomedical Engineering and Medical Physics* **2008**, *20*, 433-436, doi:10.1007/978-3-540-69367-3_116.
47. Tang, G.; Galluzzi, M.; Zhang, B.; Shen, Y.L.; Stadler, F.J. Biomechanical Heterogeneity of Living Cells: Comparison between Atomic Force Microscopy and Finite Element Simulation. *Langmuir* **2019**, *35*, 7578-7587, doi:10.1021/acs.langmuir.8b02211.
48. Alessandri, K.; Andrique, L.; Feyeux, M.; Bikfalvi, A.; Nassoy, P.; Recher, G. All-in-one 3D printed microscopy chamber for multidimensional imaging, the UniverSlide. *Scientific reports* **2017**, *7*, 42378, doi:10.1038/srep42378.